

# Tuning of the Hanle effect from EIT to EIA using spatially separated probe and control beams

Mangesh Bhattacharai, Vineet Bharti, and Vasant Natarajan\*

*Department of Physics, Indian Institute of Science, Bangalore-560012, India*

## Abstract

We demonstrate a technique for continuous tuning of the Hanle effect from electromagnetically induced transparency (EIT) to electromagnetically induced absorption (EIA) by changing the polarization ellipticity of a control beam. In contrast to previous work in this field, we use spatially separated probe and control beams. The experiments are done using magnetic sublevels of the  $F_g = 4 \rightarrow F_e = 5$  closed hyperfine transition in the 852 nm D<sub>2</sub> line of <sup>133</sup>Cs. The atoms are contained in a room temperature vapor cell with anti-relaxation (paraffin) coating on the walls. The paraffin coating is necessary for the atomic coherence to be transported between the beams. The experimental results are supported by a density-matrix analysis of the system, which also explains the observed amplitude and zero-crossing of the resonances. Such continuous tuning of the sign of a resonance has important applications in quantum memory and other precision measurements.

---

\* [vasant@physics.iisc.ernet.in](mailto:vasant@physics.iisc.ernet.in)

## I. INTRODUCTION

Interaction of light fields with multilevel atoms can result in long lived atomic coherences, which has important applications in diverse areas such as next-generation atomic clocks [1], sensitive magnetometry [2], precision measurements [3], and optical memories [4]. These experiments are usually done in vapor cells, where the presence of a buffer gas or anti-relaxation (paraffin) coating on the walls increases the coherence time and results in a narrower linewidth [5–7].

Atomic coherences have also been studied in the Hanle configuration by measuring the transmission of a probe beam as a function of magnetic field. The resulting dark resonance is called electromagnetically induced transparency (EIT), while the bright resonance is called electromagnetically induced absorption (EIA). Both EIT and EIA have been studied in the past [8, 9]. More recently, tuning from EIT and EIA has been demonstrated in  $^{87}\text{Rb}$  [10],  $^{39}\text{K}$  [11], and  $^{133}\text{Cs}$  [12]. The present work also demonstrates tuning from EIT to EIA, but is different because it uses spatially separated control and probe beams.

We further show that the experimental results are supported by a detailed density-matrix analysis of the system. The presence of spatially separated beams requires the use of a theoretical model with three regions. And the coherence survives between the two beams only when there is paraffin coating on the walls. Such spatial transport of atomic coherences is unique, and has important applications in transporting light [13], slow-light beam splitter [14] and anti-parity time symmetry [15]. The theoretical model presented in this work can also be used to provide a theoretical analysis of these experiments.

## II. EXPERIMENTAL DETAILS

A schematic diagram of the experimental setup is given in Fig. 1. The light is derived from a Toptica DL Pro laser operating near the 852 nm  $D_2$  line of  $^{133}\text{Cs}$ . The light from the laser is coupled into a polarization maintaining fiber. The light passes through a 95/5 splitter; after which 5% of it passes into a CoSY system for saturated absorption spectroscopy, and 95% of it is coupled to free space through a fiber coupler. The output beam after the coupler has a Gaussian intensity distribution with  $1/e^2$  diameter of 3 mm. The beam is passed through a half-wave retardation plate and polarizing beam splitter cube (PBS) combination, which

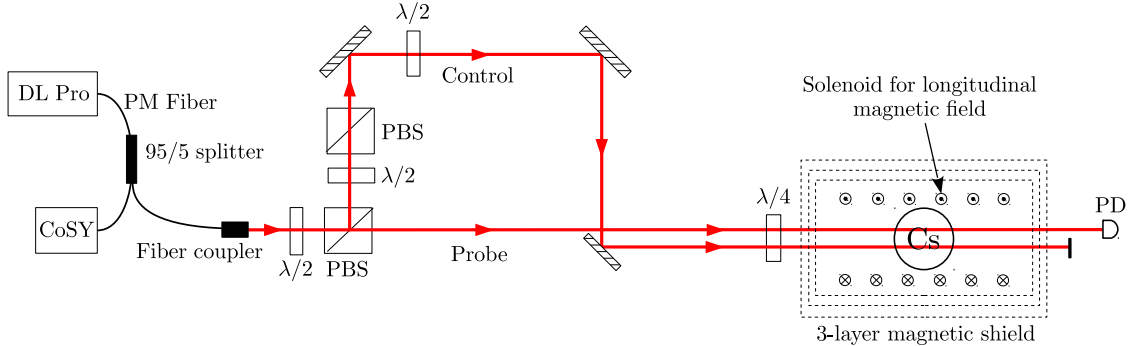


FIG. 1. Schematic of the experiment. Figure key:  $\lambda/2$  – half-wave retardation plate;  $\lambda/4$  – quarter-wave retardation plate; PM fiber – polarization-maintaining fiber, PBS – polarizing beam splitter cube; PD – photodiode.

splits the beam into the probe and control beams. The angle of the retardation plate is adjusted to control the probe power  $P_p$ . The control beam power  $P_c$  is adjusted using another half-wave retardation plate and PBS combination.

The two beams go into a spherical glass vapor cells containing  $^{133}\text{Cs}$ . The sphere has diameter of 75 mm. It has paraffin coating on the walls, which as mentioned before increases the coherence time. It is placed within a solenoid of length 640 mm and diameter 190 mm, containing 1800 turns of 0.35 mm diameter wire. The solenoid is used to apply the required longitudinal magnetic field.

The vapor cell and the solenoid are kept inside a 3-layer  $\mu$ -metal magnetic shield, which reduces stray external fields to less than 1 mG. A small residual transverse field of the order of 0.1 mG is present inside the shield. The probe beam after the shield is detected on a photodiode. The photodiode signal—which is proportional to probe transmission—is collected on the input channel of a data acquisition card. An output channel of the same card is used to sweep the current in the field-producing solenoid. The probe and control beams are parallel to each other and separated by distance of 10 mm. The ellipticity  $\epsilon$  of polarizations of the two beams is adjusted using the half-wave and quarter-wave retardation plates in their paths, as shown in the figure.

### III. THEORETICAL ANALYSIS

In this section, we develop a three-region density matrix model to analyze the spatially separated beam arrangement. Our model is based upon the multi-region model given by S. Rochester [16]. The region of interaction for atoms is divided into three regions labeled as dark, bright 1 (probe) and bright 2 (control) as shown in Fig. 2. In the dark region only magnetic field is present, whereas in the bright regions both light and magnetic field are present.

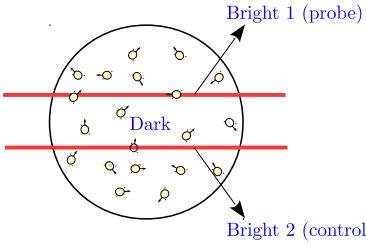


FIG. 2. Spatially separated probe and control beams used in the experiment. The regions are labeled Bright 1, Dark, and Bright 2. Atomic coherences are transported by thermal motion in the vapor cell, which survives only if there is paraffin coating on the walls.

The probe and control beams are given by the real parts of following expressions [17]

$$\begin{aligned}\mathcal{E}_p &= \mathcal{E}_{p0} \left\{ \cos \left( \epsilon_p + \frac{\pi}{4} \right) \hat{\epsilon}_{-1} - \cos \left( \epsilon_p - \frac{\pi}{4} \right) \hat{\epsilon}_{+1} \right\} e^{-i\omega_l t} \\ \mathcal{E}_c &= \mathcal{E}_{c0} \left\{ \cos \left( \epsilon_c + \frac{\pi}{4} \right) \hat{\epsilon}_{-1} - \cos \left( \epsilon_c - \frac{\pi}{4} \right) \hat{\epsilon}_{+1} \right\} e^{-i\omega_l t}\end{aligned}\quad (1)$$

Here,  $\mathcal{E}_{p0(c0)}$  and  $\epsilon_{p(c)}$  are the respective amplitude and ellipticity of probe (control) beam, and  $\hat{\epsilon}_{\mp 1}$  are the unit vectors along  $\sigma^{\mp}$  directions.

We present theoretical results for an  $F_g = 1 \rightarrow F_e = 2$  transition, which is the simplest case for  $F_g \rightarrow F_e = F_g + 1$  closed transitions. The magnetic sublevels for the  $F_g = 1 \rightarrow F_e = 2$  transition, labeled  $|1\rangle$  to  $|8\rangle$ , are shown in Fig. 3. The probe field transitions are shown with solid lines and control field transitions are shown with dashed lines. We consider that the probe beam has  $\sigma^+$  polarization and the control beam polarization is varied from  $\sigma^+$  to  $\sigma^-$  by changing its ellipticity.

The time evolution of the system for three regions is given by following set of coupled

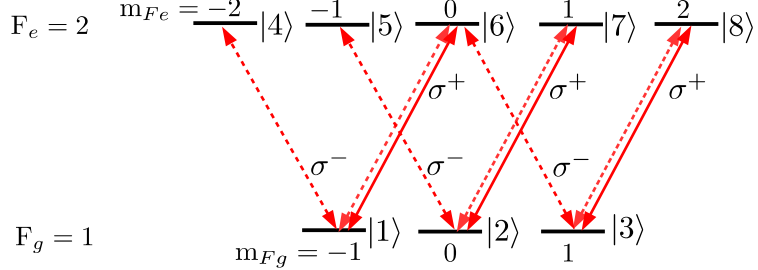


FIG. 3. Magnetic sublevels for  $F_g = 1 \rightarrow F_e = 2$  transition. The probe beam has  $\sigma^+$  polarization, and transitions coupled by it are shown with solid lines. The control beam polarization is varied from  $\sigma^+$  to  $\sigma^-$ , with transitions shown by dotted lines.

density matrix equations:

$$\begin{aligned}
\dot{\rho}^{\text{bright1}} &= \frac{-i}{\hbar} [(H_{\text{int}} + H_B), \rho^{\text{bright1}}] - \frac{1}{2} \{ \Gamma, \rho^{\text{bright1}} \} - \gamma_{t1} \rho^{\text{bright1}} + \Lambda^{\text{bright1}} + \gamma_{t1} \rho^{\text{dark}} \\
\dot{\rho}^{\text{dark}} &= \frac{-i}{\hbar} [H_B, \rho^{\text{dark}}] - \frac{1}{2} \{ \Gamma, \rho^{\text{dark}} \} + \frac{\gamma_{t2}}{2} (\rho^{\text{bright1}} + \rho^{\text{bright2}}) + \Lambda^{\text{dark}} - (\gamma_{t2} + \gamma_w) \rho^{\text{dark}} \\
&\quad + \frac{\delta^{\text{gs}}}{2F_g + 1} \gamma_w \\
\dot{\rho}^{\text{bright2}} &= \frac{-i}{\hbar} [(H_{\text{int}} + H_B), \rho^{\text{bright2}}] - \frac{1}{2} \{ \Gamma, \rho^{\text{bright2}} \} - \gamma_{t3} \rho^{\text{bright2}} + \Lambda^{\text{bright2}} + \gamma_{t3} \rho^{\text{dark}}
\end{aligned} \tag{2}$$

where  $H_{\text{int}}^{\text{bright1}}$  and  $H_{\text{int}}^{\text{bright2}}$  are the Hamiltonian for light-atom interaction in bright 1 and bright 2 regions,  $\Gamma$  is the relaxation matrix for decay of atoms from excited levels due to spontaneous emission,  $\Lambda^{\text{bright1,bright2,dark}}$  represent repopulations of atoms in the ground levels due to decay from excited levels in bright 1, bright 2 and dark regions,  $\gamma_w$  is ground state relaxation rate due to wall collisions,  $\gamma_{t1}$  is the transit relaxation from bright 1 to dark region,  $\gamma_{t2}$  is the transit relaxation from dark region to the bright regions, and  $\gamma_{t3}$  is the transit relaxation from bright 2 to dark region, and  $\delta^{\text{gs}}$  is the identity matrix for ground state.

The light-atom interaction Hamiltonians for the bright 1 and bright 2 regions can be described as:

$$H_{\text{int}}^{\text{bright1}} = \frac{\hbar}{2} \sum_{i=1}^3 \sum_{j=4}^8 |i\rangle \langle j| \Omega_{ij}^p \left[ \cos \left( \epsilon_p + \frac{\pi}{4} \right) \delta_{i+3,j} + \cos \left( \epsilon_p - \frac{\pi}{4} \right) \delta_{i+5,j} \right] + \text{h.c.} \tag{3}$$

$$H_{\text{int}}^{\text{bright2}} = \frac{\hbar}{2} \sum_{i=1}^3 \sum_{j=4}^8 |i\rangle \langle j| \Omega_{ij}^c \left[ \cos \left( \epsilon_c + \frac{\pi}{4} \right) \delta_{i+3,j} + \cos \left( \epsilon_c - \frac{\pi}{4} \right) \delta_{i+5,j} \right] + \text{h.c.} \tag{4}$$

The magnetic field Hamiltonian can be described as:

$$H_B = \mu_B B_z \begin{bmatrix} g_F \sigma_{3 \times 3}^{(z)} & 0 \\ 0 & g_{F'} \sigma_{5 \times 5}^{(z)} \end{bmatrix} + \mu_B B_x \begin{bmatrix} g_F \sigma_{3 \times 3}^{(x)} & 0 \\ 0 & g_{F'} \sigma_{5 \times 5}^{(x)} \end{bmatrix} \quad (5)$$

where  $B_z$  is the longitudinal component of the magnetic field,  $B_x$  is the residual component of the transverse field,  $g_F$  is the Landè g-factor of the ground level,  $g_{F'}$  is the Landè g-factor of the excited level,  $\mu_B$  is Bohr magneton, and  $\sigma_{2i+1 \times 2i+1}^{(x)}$  and  $\sigma_{2i+1 \times 2i+1}^{(z)}$  are the  $x$  and  $z$  components of Pauli matrices for spin  $i$  particles.

## IV. RESULTS AND DISCUSSION

### A. Transformation from EIT to EIA

Spectra for Hanle resonances for the  $F_g = 4 \rightarrow F_e = 5$  transition are shown in Fig. 4. We show probe transmission versus longitudinal magnetic field for different values of control field ellipticity. The ellipticity of the probe beam is fixed at  $+45^\circ$  and the ellipticity of the control beam is varied from  $+45^\circ$  to  $-45^\circ$  in the steps of  $10^\circ$ . Part (a) shows the experimental spectra, and part (b) shows the theoretical spectra. The Hanle resonance peak shows increased transmission (or EIT) for same handedness of circular polarized beams, which changes to reduced transmission (or EIA) for opposite handedness. The transformation is continuous with change in ellipticity of the control beam, as seen from the figure. The resonances are not centered at zero field because of the presence of a small residual field inside the shield. The experimental spectra are obtained using powers of  $30 \mu\text{W}$  in the probe field and  $80 \mu\text{W}$  in the control field. As shown in the next section, a control power greater than the probe power is required for the transformation from EIT to EIA to occur.

The theoretical analysis is done by assuming that the atoms have no velocity distribution. In addition, the intensities in the probe and control fields are assumed to be constant. Both these assumptions imply that the Rabi frequencies necessary to reproduce the experimental results are smaller than those at the center of the two Gaussian beams used for the experimental data, namely  $30 \mu\text{W}$  and  $80 \mu\text{W}$  respectively. This point is described in detail in the work of Renzoni *et al.* [18] and discussed in the appendix.

The use of a paraffin-coated vapor cell has two effects. One is that the resonances are much narrower compared to previous work in this field. The second effect, and one that is

more important to the work here, is that the transport of atomic coherences with spatially separated beams is only possible in such a cell [13–15].

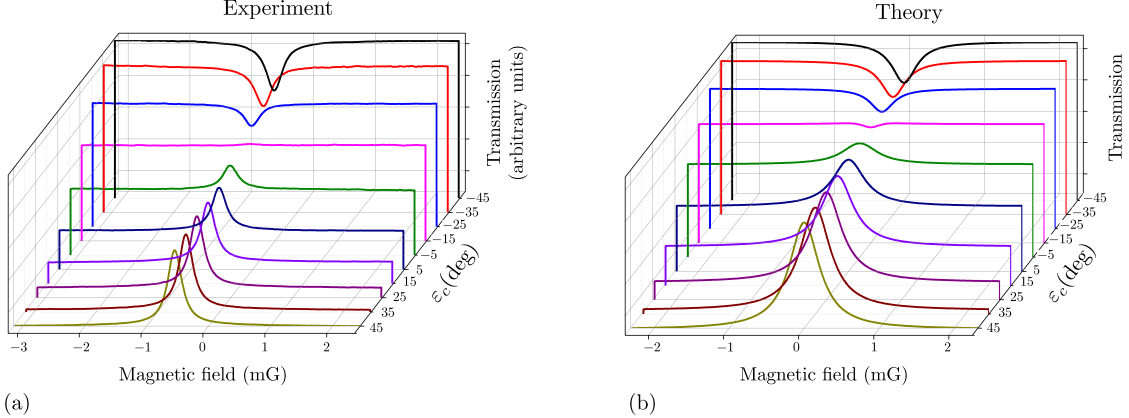


FIG. 4. Transformation from EIT to EIA with change in control ellipticity.  $\epsilon_p$  is kept fixed at  $+45^\circ$ , while  $\epsilon_c$  is varied from  $+45^\circ$  to  $-45^\circ$ . Part (a) shows the experimental spectra. Part (b) shows the theoretical results, with the ratio of the probe and control Rabi frequencies same as that in the experiment. Values of various relaxation rates as defined in the theoretical analysis section are as follows: (i)  $\gamma_{t1} = \gamma_{t3} = 0.012\Gamma$ , (ii)  $\gamma_{t2} = 0.00003\Gamma$ , and (iii)  $\gamma_w = 0.000005\Gamma$ .

## B. Effect of control power on the amplitude of the resonances

In this section, we discuss the effect of control field power on the amplitude of the Hanle resonances. The resonances for probe transmission are analyzed by fitting the peaks about the line center using a Lorentzian function:

$$L = \frac{A}{(B - B_0)^2 + \Gamma^2/4} \quad (6)$$

The amplitude of resonance—peak height from the baseline—is given by  $4A/\Gamma^2$ . The experiments are performed for a fixed probe power of  $P_p = 30 \mu\text{W}$ . The control power  $P_c$  is varied to get the four ratios shown in Fig. 5. The theoretical results, shown in part (b) of the figure, are scaled to roughly match the experimental data. Note that the ratios of Rabi frequencies is equal to the square root of the power ratios. The theoretical results match the experimental data quite well. This control over the amplitude of narrow resonances implies that the medium can be tuned between sub- and super-luminal light propagation simply by changing the ellipticity of the control beam [19].

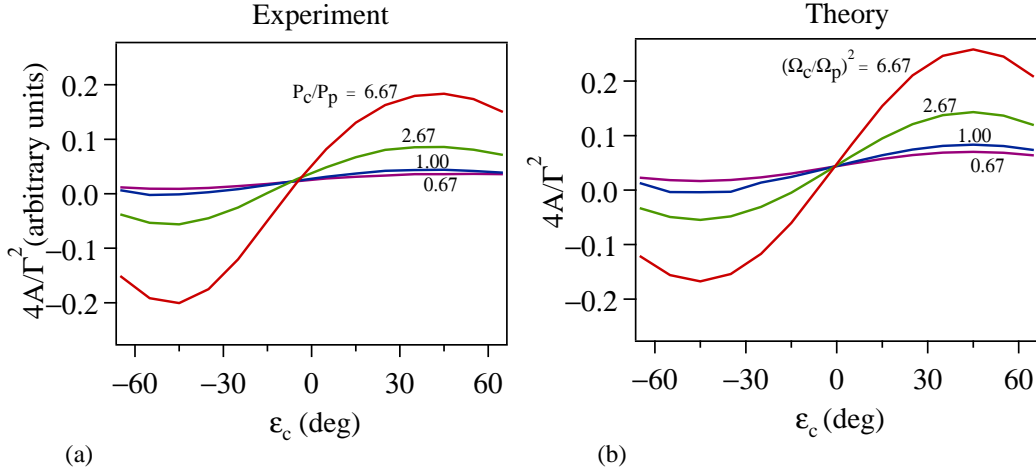


FIG. 5. Amplitude of the resonance (as defined in the text) as a function of control ellipticity for 4 values of control power. The probe power is fixed at 30  $\mu\text{W}$ , and the values of control power are given in terms of power ratios. Part (a) shows the experimental results while part (b) shows the theoretical results. Note that the ratio of Rabi frequencies is equal to the square root of the powers.

### C. Zero crossing of the resonance

The experimental spectra show that the transformation from EIT to EIA, i.e. where the amplitude of the resonance is zero, does not happen at a value of  $\epsilon_c = 0$ . We have therefore studied the value of  $\epsilon_c$  where the transformation occurs. The results are shown in Fig. 6 for different values of power ratios. The important thing to note is that the theoretical values match the experimental values quite well. Qualitatively, this can be understood as arising due to optical pumping among the magnetic sublevels shown in Fig. 3. When the probe and control beams both have  $\sigma^+$  polarizations (parallel), then population gets pumped into the  $|3\rangle$  level. For any other polarization, the control beam will have both  $\sigma^+$  and  $\sigma^-$  components. Whenever  $\sigma^-$  transition strength is larger than  $\sigma^+$  transition (contributed by probe and corresponding component of control), the population gets pumped into the  $|1\rangle$  level. This explanation tells us that for a particular value of  $\epsilon_c$  ( $\neq 0$ ) the Hanle resonance transforms from EIT to EIA. This also implies that the control power has to be larger for the transformation to occur.

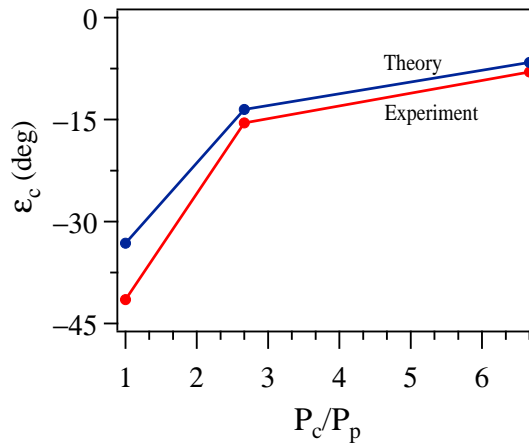


FIG. 6. Theoretical and experimental values of the zero point of the Hanle resonance as a function of control power. For ease of comparison to other data, the control power is given as a ratio.

## V. CONCLUSIONS

In summary, we demonstrate a technique of tuning Hanle resonances from EIT to EIA, using spatially separated probe and control beams. The experiments are done using magnetic sublevels of the closed  $F_g = 4 \rightarrow F_e = 5$  transition in the D<sub>2</sub> line of <sup>133</sup>Cs. The atoms are contained in a room temperature vapor cell, with paraffin coating on the walls. Such coating is important for atomic coherences to be maintained between the spatially separated beams.

The requirement for EIT is that the two beams have same circular polarizations. The peak transforms to EIA when the polarizations are orthogonal. The transformation occurs only when the control power is much larger than the probe power. We have verified this by studying the transformation for different ratios of powers. The experimental results are explained by a theoretical density-matrix analysis of the sublevels involved in the transition. The model is also able to explain the observed value of control ellipticity where the transformation from EIT to EIA occurs.

The ability to control Hanle resonances from enhanced transmission to enhanced absorption make this a good technique for sensitive magnetometry and control over group velocity.

## ACKNOWLEDGEMENTS

This work was supported by the Council of Scientific and Industrial Research, India. The authors thank Sumanta Khan, Jay Mangaonkar, and Disha Kapasi for help with the experiments; and S Raghuveer for help with the manuscript preparation.

## APPENDIX

In this appendix, we discuss the method to approximate the Rabi frequencies for theoretical analysis. The saturation intensity ( $I_s$ ) is not the same for atoms moving with different longitudinal velocities.

The population of excited state after the interaction of atoms with light is given as:

$$\rho_{22} = \frac{\Omega^2/4}{\delta^2 + \Omega^2/2 + \Gamma^2/4} \quad (7)$$

where  $\delta$  is the detuning of light from resonance,  $\Omega$  is the Rabi frequency, and  $\Gamma$  is the natural linewidth of excited state.

For light field on resonance ( $\delta = 0$ ) and atoms moving with  $v$ , Eq. (7) can be written as:

$$\rho_{22}(v) = \frac{\Omega^2/4}{(kv)^2 + \Omega^2/2 + \Gamma^2/4} \quad (8)$$

The excited state population by considering Maxwell-Boltzmann (MB) velocity distribution of atoms is

$$\rho_{22} = \int_{-\infty}^{+\infty} \rho_{22}(v) f(v) dv, \quad (9)$$

where

$$f(v) = \sqrt{\frac{m}{2\pi k_B T}} \exp\left(\frac{-mv^2}{2k_B T}\right) \quad (10)$$

We solve for the  $\Omega/\Gamma$  at saturation by equating Eq. (9) to 1/4. In our theoretical model, we have ignored the longitudinal velocity distribution. Therefore, the effective Rabi frequency for the model assuming atoms with zero longitudinal velocities—calculated by assuming the ratio  $I/I_s$  is same for both model and experiment—is given as

$$(\Omega/\Gamma)_{\text{model}} = \frac{1}{\sqrt{2}} \frac{(\Omega/\Gamma)_{\text{expt}}}{(\Omega/\Gamma)_{I_s, \text{MB}}} \quad (11)$$

## AUTHOR CONTRIBUTIONS

VN conceived the study; MB did the experiments; MB and VB did the theoretical simulation; all authors reviewed the manuscript for intellectual content, and read and approved the final version.

---

- [1] J. Vanier, *Appl. Phys. B: Lasers and Optics* **81**, 421 (2005), 10.1007/s00340-005-1905-3.
- [2] D. Budker, W. Gawlik, D. F. Kimball, S. M. Rochester, V. V. Yashchuk, and A. Weis, *Rev. Mod. Phys.* **74**, 1153 (2002).
- [3] A. Krishna, K. Pandey, A. Wasan, and V. Natarajan, *Europhys. Lett.* **72**, 221 (2005).
- [4] A. I. Lvovsky, B. C. Sanders, and W. Tittel, *Nat. Photon.* **3**, 706 (2009).
- [5] S. Brandt, A. Nagel, R. Wynands, and D. Meschede, *Phys. Rev. A* **56**, R1063 (1997).
- [6] M. A. Bouchiat and J. Brossel, *Phys. Rev.* **147**, 41 (1966).
- [7] H. Ravi, M. Bhattacharai, Y. D. Abhilash, U. Momeen, and V. Natarajan, *Asian J. Phys.* **25**, 1093 (2016).
- [8] F. Renzoni, W. Maichen, L. Windholz, and E. Arimondo, *Phys. Rev. A* **55**, 3710 (1997).
- [9] F. Renzoni, C. Zimmermann, P. Verkerk, and E. Arimondo, *Journal of Optics B: Quantum and Semiclassical Optics* **3**, S7 (2001).
- [10] N. Ram and M. Pattabiraman, *Journal of Physics B: Atomic, Molecular and Optical Physics* **43**, 245503 (2010).
- [11] S. Gozzini, A. Fioretti, A. Lucchesini, L. Marmugi, C. Marinelli, S. Tsvetkov, S. Gateva, and S. Cartaleva, *Opt. Lett.* **42**, 2930 (2017).
- [12] H. Ravi, M. Bhattacharai, V. Bharti, and V. Natarajan, *EPL (Europhysics Letters)* **117**, 63002 (2017).
- [13] A. S. Zibrov, A. B. Matsko, O. Kocharovskaya, Y. V. Rostovtsev, G. R. Welch, and M. O. Scully, *Phys. Rev. Lett.* **88**, 103601 (2002).
- [14] Y. Xiao, M. Klein, M. Hohensee, L. Jiang, D. F. Phillips, M. D. Lukin, and R. L. Walsworth, *Phys. Rev. Lett.* **101**, 043601 (2008).
- [15] P. Peng, W. Cao, C. Shen, W. Qu, J. Wen, L. Jiang, and Y. Xiao, *Nature Physics* **12**, 1139 (2016).
- [16] S. M. Rochester, Ph.D. thesis (2010).

- [17] M. Auzinsh, D. Budker, and S. M. Rochester, *Optically Polarized Atoms*.
- [18] F. Renzoni, S. Cartaleva, G. Alzetta, and E. Arimondo, Phys. Rev. A **63**, 065401 (2001).
- [19] V. Bharti and V. Natarajan, Optics Communications **392**, 180 (2017).